



# Experimental investigation of true triaxial unloading rockburst precursors based on critical slowing-down theory

Jieyu Li<sup>1,2</sup> · Dongqiao Liu<sup>1</sup> · Manchao He<sup>1</sup> · Yunpeng Guo<sup>1</sup> · Haosen Wang<sup>1,2</sup>

Received: 15 October 2022 / Accepted: 30 January 2023 / Published online: 9 February 2023  
© Springer-Verlag GmbH Germany, part of Springer Nature 2023

## Abstract

Rockburst warnings are a significant problem in the field of rock engineering. In this study, a rockburst experimental system was developed to conduct a true triaxial single-side rapid unloading rockburst experiment. The rockburst process and time were recorded using a high-speed camera. Based on the critical slowing-down theory, the acoustic emission (AE)  $RA/AF$ , duration, and rise time in the rockburst process were studied to obtain rockburst precursor information. The main conclusions of the experiment are as follows. (1) In the early stage of rockburst, the AE signal appears to be a critical-slowness phenomenon at the critical point, which is manifested as an increase in the variance and autocorrelation coefficient, and it also appears in the increase in the variance and autocorrelation coefficient during rapid unloading. A recording made using a high-speed camera shows that the rockburst occurrence time does not necessarily correspond to the peak stress point of the stress–strain curve. (2) The variances in the AE  $RA/AF$  value, duration, and rise time are the same. The sudden change time of the precursor signal is the same, the waveform fluctuation is similar, and they all appear before the rockburst. At this time, the AE localization event shows that many high-energy events occur in the sandstone, and cracks appear on the sandstone surface. (3) The autocorrelation coefficient fluctuates considerably compared with the variance; therefore, the variance can be considered the main criterion for rockburst precursors. This study provides a theoretical basis for predicting rockbursts.

**Keywords** Rockburst experiment · Rockburst warning · Acoustic emission (AE) · Critical slowing-down theory · AE localization

## Introduction

Hydropower construction projects, mining of mineral resources, and geological disposal of nuclear waste involve deep rock excavation. A rockburst is a sudden failure phenomenon during the excavation of a deep high-stress rock mass, which often causes severe damage to the excavation face, equipment damage, and casualties. It is one of the most severe disasters encountered in the excavation of deep rock mass engineering (Cook 1963; Kaiser and Cai 2012; He et al. 2019; Gong et al. 2022). Predicting

rockbursts is an urgent technical problem for safety during deep rock mass engineering. Owing to various limitations, it is difficult to conduct in situ rockburst research. Using indoor rockburst simulation mechanical tests, rock mass fracture instability and rockburst can be studied effectively. Currently, rock mechanics researchers generally simulate rockbursts using true triaxial loading for rapid one-sided unloading. Substantial rockburst research has been conducted using this experimental method (He et al. 2012; Du et al. 2016; Gong et al. 2018).

Before a rockburst occurs, a large amount of information is released. The critical issue is to use this precursory information reasonably for adequate early warning. The generation principle of acoustic emission (AE) is that, when a rock mass is subjected to an external load, local stress changes, microcracks form in the rock mass, and some of the deformation energy is released in the form of elastic waves (Lockner 1993; Hardy 1972). AE contains a large amount of information, including the damage degree of the rock mass and evolution of internal cracks (Gong et al. 2019;

✉ Dongqiao Liu  
liudongqiao@yeah.net

<sup>1</sup> State Key Laboratory for GeoMechanics and Deep Underground Engineering, China University of Mining and Technology, Beijing 100083, China

<sup>2</sup> Norman B. Keevil Institute of Mining Engineering, University of British Columbia, Vancouver, BC V6T 1Z4, Canada

Wu et al. 2021; Wang et al. 2022; Liu et al. 2022). Many researchers have investigated the characteristics of AE rock failure and rockburst precursors based on AE technology. Li et al. (2021) performed uniaxial loading experiments on sandstone with different water contents and conducted multifractal analysis of AE signals and found that multifractal parameters suddenly increased by  $\Delta\alpha$ , and the sudden decrease of  $\Delta f$  in the time series can be used as a precursor of rock instability and failure. Wang et al. (2021) analyzed the AE main frequency entropy during rockburst evolution by conducting true triaxial single-sided granite rockburst experiments and found that the main AE frequency entropy decreased significantly before the rockburst. Luo et al. (2022) performed Brazil splitting, direct shear, uniaxial, and biaxial compression tests on natural and saturated sandstone samples. They monitored the entire failure process of each sample using an MS system combined with an AE system. It was found that a significant sudden increase in the fractal dimension and significant sudden decrease in  $b$  value typically indicated that the rock would break immediately. Li and Xu (2021) introduced the Hurst index into geotechnical engineering and used it to study rock failure. The results show that the Hurst index starts to decline and an increase in the AE parameters can be used as an early-warning point for rock instability. Dong et al. (2021) studied the qualitative relationship between the precursor of rock instability and the direction of the principal stress through rock AE and wave velocity. The experiment shows that the AE event rate and wave velocity exhibit stable changes in the elastic stage of rock samples and unstable changes in the plastic stage implying that the AE event rate and wave velocity can be used to monitor the parameters for rock instability. Many researchers have conducted studies on the AE precursory characteristics of rock fracture and rockbursts; however, a better method for studying the AE characteristics of precursory rockbursts must be developed.

For complex dynamic systems in nature, the transition from one state to another is a universal phenomenon. When the system approaches the critical transition period, a phenomenon called “critical slowing” appears, manifested as an increase in the signal variance and autocorrelation coefficient. This phenomenon is a crucial transition feature of complex dynamic systems and has been applied in many fields (Scheffer et al. 2009; Gopalakrishnan et al. 2016), including ecosystems (Beck et al. 2018), climate systems (Dakos and Scheffer 2008), earthquake prediction (Ramos 2010), and disease prediction in medicine (Venegas et al. 2005). Therefore, before a sudden change in the system, the critical deceleration characteristics of various power systems are everywhere and can be regarded as early-warning signals. Some researchers have conducted relevant research on the precursory characteristics of rock failure based on critical-slowness theory. Wei et al. (2018) analyzed AE

counts using the critical-slowness theory and found that the variance and autocorrelation coefficient of the AE count increased when the rock sample entered the crucial state of failure. The sudden increase in the autocorrelation coefficient and variance of the AE count could be considered a precursory information of rock failure. Zhang et al. (2019) found that the precursory information obtained using the charge signal occurred earlier in the time series than the AE count. Zhang et al. (2021) added an analysis of the AE energy and  $RA$  values based on previous studies on AE ring counting. They found that the above parameters also exhibit the critical-slowness characteristics. Zhu et al. (2022) studied the critical-slowness phenomenon of AE  $RA/AF$  characteristics, duration, rise time, and other multicharacteristic parameters based on the critical-slowness theory. Although significant work has been done in predicting rock failure through critical slowness-down theory, the experiments were limited to uniaxial rock compression experiments. Because rockburst is an engineering disaster problem caused by the stress concentration resulting from the excavation unloading of rock mass in a three-dimensional in situ stress state, the uniaxial compression experiment cannot reflect the excavation unloading, three-dimensional stress state, and mechanical boundary. Thus, no relevant research has been reported on the experimental prediction of rockbursts based on critical-slowness theory. Additionally, AE localization to reflect the internal crack characteristics of rock corresponding to the critical-slowness phenomenon was not considered in those studies.

In this study, true triaxial single-sided rapid unloading under high pressure was performed, using a self-developed true triaxial rockburst experimental system to simulate rockbursts, and high-speed cameras were used to capture the rockbursts. Based on the critical-slowness theory, the AE precursor characteristics of rockbursts were studied. The microcrack evolution in rock corresponding to the critical-slowness phenomenon was studied by employing AE localization technology.

## Experimental procedures and theory

### Experiment samples and rockburst system

Fine-grained red sandstone (Fig. 1) with a high homogeneity was used in the experiment. It was a 150-mm cube, and its six faces were carefully polished to prevent end effects during loading. Figure 2 depicts a 77 $\times$  scanning electron microscopy (SEM) image of the sandstone sample. SEM observations indicated that the sandstone sample was an inhomogeneous porous material. Tables 1 and 2 list the relative contents of the whole rock and clay mineral composition of the sandstone used in the experiment, respectively.

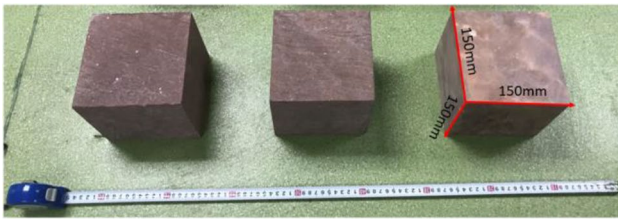


**Fig. 1** Sandstone sample

The main minerals were plagioclase, quartz, clay, and small amounts of potassium feldspar, calcite, hematite, and laumontite. The clay minerals were mainly composed of green montmorillonite and illite. To avoid dispersion of the experimental data, the true triaxial unloading rockburst precursor information experiment was performed thrice.

The true triaxial rockburst experimental system used in the experiment was from a new generation of rockburst experimental systems independently developed by the State Key Laboratory for GeoMechanics and Deep Underground Engineering, China University of Mining and Technology (Beijing), as shown in Fig. 3a. The rockburst experimental equipment had three independent loading systems that were perpendicular to each other. During the loading process, multiple loading surfaces in the horizontal direction could be quickly unloaded to form free surfaces to simulate the excavation process in underground projects by blasting and, subsequently, reproduce the rockburst damage phenomenon (He et al. 2021). The maximum axial and horizontal loading forces of the experimental system were 5000 and 2000 kN, respectively. The experimental system was equipped with a high-speed camera (Fig. 3b, c) that accurately captured the time and process of the rockburst to determine the advance time of the rockburst precursor information and an AE monitoring equipment to monitor the crack evolution process and AE precursor information characteristics of rockbursts. The AE monitoring equipment was a PAC Micro II system (Fig. 3d) with a maximum signal amplitude of 100 dB and

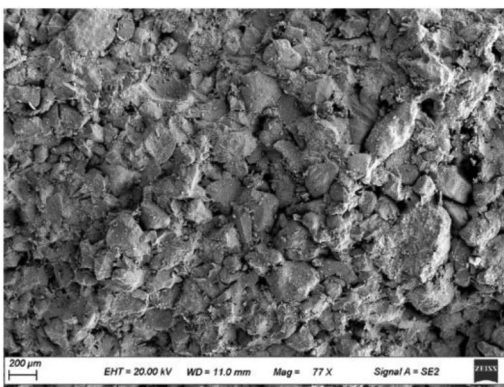


**Fig. 2** Sandstone scanning electron microscope (SEM) photo

maximum sampling rate of 40 Msps, and the probe used was a nano-30 sensor (Fig. 3e). During the rockburst experiment loading process, the AE signal acquisition threshold was set to 45 dB, and sampling interval was set to 1  $\mu$ s. To explore the critical-sliding precursory characteristics of sandstone rockbursts, AE positioning technology was used to reflect the internal cracks in sandstones corresponding to the precursory characteristics of rockbursts. Eight AE probes were used in the experiment, and their specific positions on the fixture are shown in Fig. 4.

## Experimental method

Deep rock mass rockbursts are mainly caused by excavation under high pressure. After excavation, the radial stress of the surrounding rock of the roadway decreases to zero, and tangential stress concentrates owing to the new distribution of the excavation stress. As shown in Fig. 5a, when the stress concentration exceeds the strength of the surrounding rock, the elastic strain energy accumulated in the surrounding rock is released instantly, causing a rockburst. Currently, the method of excavating rock mass in deep underground engineering is typically done by blasting excavation, which is a rapid unloading process (Yang et al. 2016). The deep unexcavated rock mass is in a three-dimensional stress state, and true triaxial equipment simulates three-dimensional stress loading. Simulate blasting excavation by rapid unloading. After unloading, the axial stress was increased to simulate the stress concentration after excavation until the rockburst (He et al. 2020).

Figure 5b shows the true triaxial stress loading path of the rockburst experiment. First, the triaxial stress was loaded to the designed initial stress state of the original rock and was maintained for some time such that the triaxial pressure was applied stably to the experimental sample. After the unloading was completed, the loading surface stress  $\sigma_{31}$  in the direction of the minimum principal stress was quickly unloaded (when the sandstone is exposed to the free surface after the unloading is completed, and the high-speed camera was turned on to capture the change in the free surface). After the unloading is completed, the axial direction stress  $\sigma_1$  was increased until the rockburst occurred. When the loading surface stress  $\sigma_{31}$  was unloaded in the  $\sigma_3$  direction, the relative loading surface stress  $\sigma_{32}$  decreased to a small value, but not zero, because the action force is equal to the reaction force. This minor stress was due to the frictional force caused by the loading stress in the other two directions. Additionally, this small stress corresponds to the still small pressure in the rock mass near the on-site face, which is perpendicular to the direction of the face. In this study, the initial in situ loading stresses  $\sigma_1$ ,  $\sigma_2$ , and  $\sigma_3$  were 30.7, 25.7, and 19 MPa,

**Table 1** Relative content of mineral components for sandstone

Mineral content (%)						
Quartz	Potash feldspar	Plagioclase	Calcite	Hematite	Laumontite	Clay mineral
16.0	4.2	68.6	2.8	1.3	2.1	5.0

respectively. Force loading was used in this experiment at a loading speed of 2 kN/s.

The rockburst experiment simulated the stress transformation path consistent with the field, and the results should correspond to a real rockburst. Figure 6 shows a comparison between the rockburst experiment and an on-site rockburst. Figure 6a shows the ejection process of the rockburst fragments captured by a high-speed camera. First, cracks are present on the rock surface, the fragments peel off from the surface that then jet to the free face, and finally, a rockburst pit is formed. The figure shows that the rockburst pit is V-shaped. Figure 6b shows a photograph of the experimental rockburst sample after destruction. The sample has two macro shear cracks and a V-shaped pit. Figure 6c shows fragments ejected by a rockburst, mainly in a sheet shape. Figure 6d shows photographs of the on-site rockburst. The rockburst pit was V-shaped, and most rockburst fragments were sheet-shaped. The experimental rockburst test results agree well with the field results.

**Principle of the critical slowing-down theory**

In a natural dynamic system, if the phase state of the system changes (that is, when the system varies from an old phase state to a new phase state), there are scattered fluctuations near the adjacent point that are conducive to the formation of the new phase state, which is manifested as an increase in amplitude and extension of the fluctuation time. After the disturbance, the recovery speed becomes slower, and the ability to recover to the old phase decreases. This phenomenon is known as “critical slowing” (Scheffer et al. 2009; Kong et al. 2015; Gopalakrishnan et al. 2016). This phenomenon is often observed using variance and autocorrelation coefficients. When the phase state of the system changes, the variance and autocorrelation coefficients show an increasing trend. Variance is a characteristic quantity that describes the

degree of deviation of the data from the average value in a sample and can be expressed as

$$S^2 = \frac{1}{n} \sum_i^n (x_i - \bar{x})^2 \tag{1}$$

where  $S^2$  is the variance,  $x_i$  is the  $i$ -th data point, and  $\bar{x}$  is the average.

The autocorrelation coefficient is a statistic that describes the correlations between the same variables at different times. The autocorrelation coefficient with  $x$  lag length  $j$  can be expressed as,

$$a(j) = \sum_{i=1}^{n-j} \left( \frac{x_i - \bar{x}}{s} \right) \left( \frac{x_{i+j} - \bar{x}}{s} \right) \tag{2}$$

Assuming that there is a forced disturbance with a period  $\Delta t$  of the state variable, during the disturbance process, the recovery rate is  $\lambda$ , which is an approximately exponential relationship that can be described in the regression model as,

$$y_{n+1} = e^{\lambda \Delta t} y_n + s \epsilon_n \tag{3}$$

where  $y_n$  is the deviation of the system variable from the equilibrium state and  $\epsilon_n$  is a random quantity conforming to the normal distribution. If  $\lambda$  does not depend on  $y_n$ , the process can be simplified to

$$y_{n+1} = a y_n + s \epsilon_n \tag{4}$$

where  $a$  is the autocorrelation coefficient and  $a = e^{\lambda \Delta t}$ . Equation (4) can be obtained by analyzing the variance,

$$Var(y_{n+1}) = E(y_n^2) + [E(y_n)]^2 = \frac{s^2}{1 - a^2} \tag{5}$$

Here,  $E$  is the mathematical expectation value.

When the system approaches the critical point, the recovery rate  $\lambda$  caused by its disturbance decreases and approaches zero, autocorrelation coefficient  $a$  approaches 1, and variance approaches infinity. Therefore, increasing the

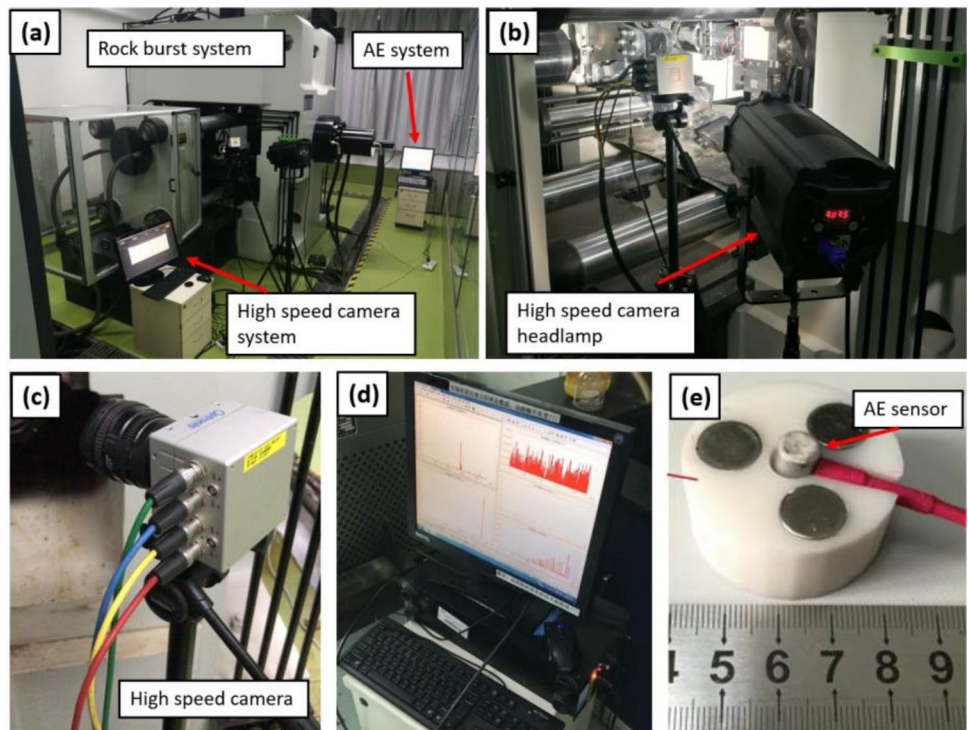
**Table 2** Relative content of clay mineral components for sandstone

Relative content of clay minerals (%)						Mixed layer ratio (%S)	
<i>S</i>	<i>I/S</i>	<i>It</i>	<i>Kao</i>	<i>C</i>	<i>C/S</i>	<i>I/S</i>	<i>C/S</i>
/	/	16	/	/	84	/	50

*S* smectites, *I/S* Imon mixed layer, *It* illite, *K* kaolinite, *C* chlorite, *C/S* green smectite layer



**Fig. 3** Rockburst system and data acquisition system. **a** True triaxial rockburst experiment system, **b** high-speed camera headlamp, **c** high-speed camera, **d** AE system, and **e** AE sensor



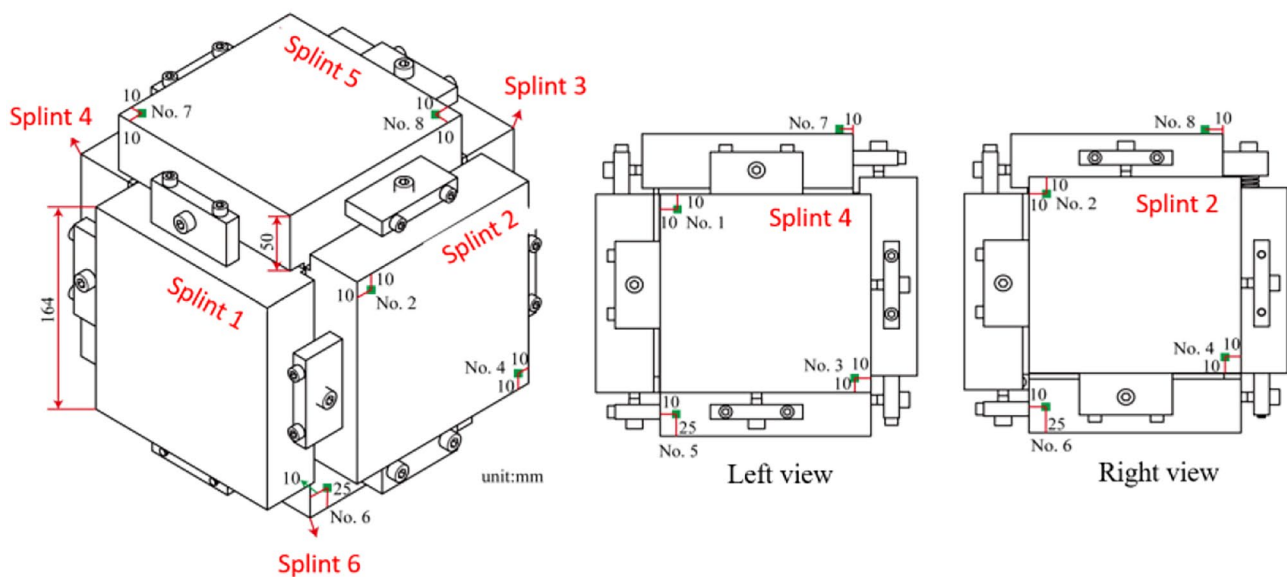
variance and autocorrelation coefficient can be a precursor to a system approaching a critical point.

## Results and discussion

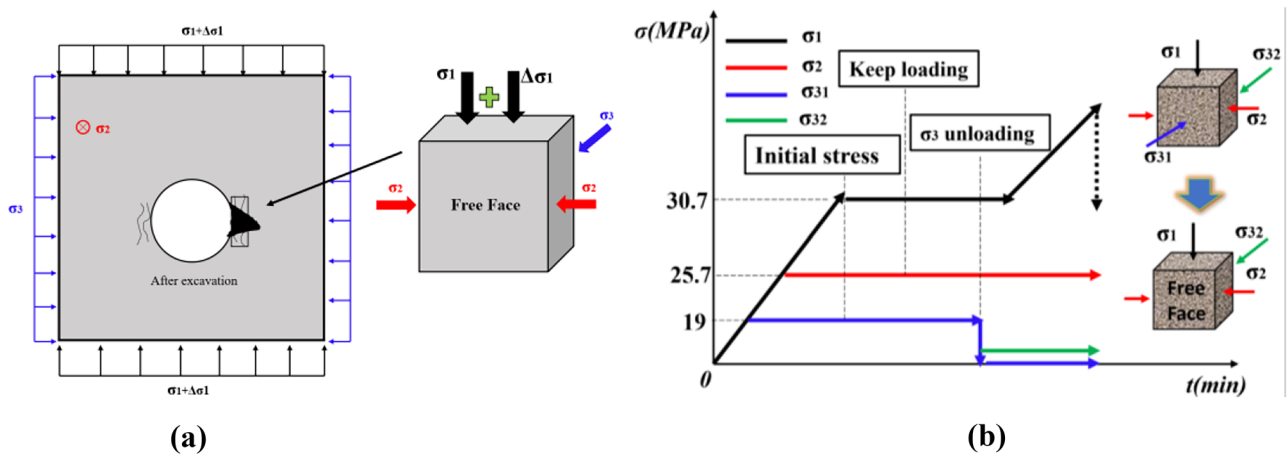
### Analysis of stress–strain

Figure 7 shows the axial stress–strain curve of the three groups of sandstone true triaxial unloading rockburst experiments.

The curve can be divided into four stages: the initial compaction, linear elasticity, yield, and postpeak stage. An unloading platform is present in the stress–strain curve at the unloading point, which differs from that of the uniaxial compression of rock and loading experiments without rapid unloading. The unloading platform is considered to be resulted from the rapid unloading of the minimum principal stress during true triaxial loading, and the sandstone is considered to expand rapidly in the unloading direction. The axial direction of the sandstone



**Fig. 4** Location of AE probe



**Fig. 5** Stress state of surrounding rock after excavation and loading path of rockburst test. **a** Stress state of surrounding rock after excavation and **b** loading path of rockburst test

sample is shortened due to the Poisson effect; therefore, the strain on the stress–strain curve suddenly increases when the axial stress is unchanged. After rapid unloading, numerous tension cracks are generated near the free face of the rock. The tension cracks continue to expand owing to the Poisson effect of the rock mass until they are connected to form plate cracking. The figure shows that the yield stages of the axial stress–strain curves of the three groups of experiments are relatively short, exhibiting strong brittle characteristics. The pentagram and dot in the curve correspond to the yield and rockburst points, respectively.

The acquisition frequency of the high-speed camera in this experiment was 1000 frames per second (that is, 1000 photographs were recorded in 1 s). The frequency of the rockburst loading equipment to collect stress and

strain data was set to 1000 groups per second. High-speed camera, rockburst equipment, and AE equipment times were unified before the experiment. The rockburst time recorded by the high-speed camera was used to obtain the corresponding stress and strain data of the loading equipment at the time point of rockburst. The peak of the sandstone axial stress was not necessarily the time point of the rockburst. Only the stress peak point of sandstone S-1 was the corresponding rockburst time point, whereas the rockburst time points of the other two sandstones were after the peak point. We believe that the rock was destroyed after it reached its peak stress. The rock fragments had a more significant acceleration at this time, but the speed was zero. When the stress drops, the rock fragments have a certain speed, and rockbursts occur. The yield point indicates that

**Fig. 6** Comparison between rockburst experiment results and on-site rockburst. **a** Ejection process of rockburst, **b** photo of rockburst sample failure, **c** rockburst experiment fragments, and **d** on-site rockburst photo (Liu et al. 2018)

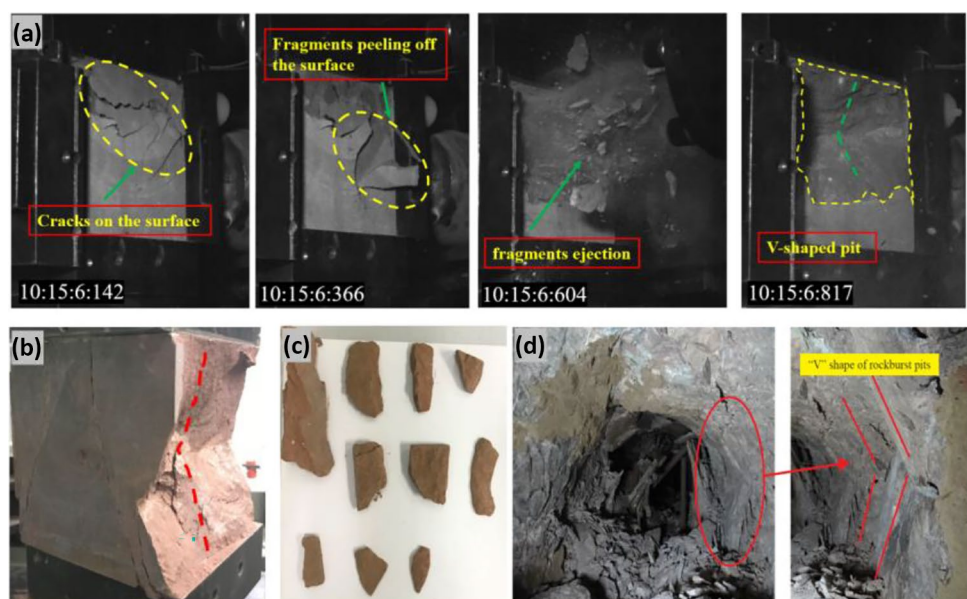
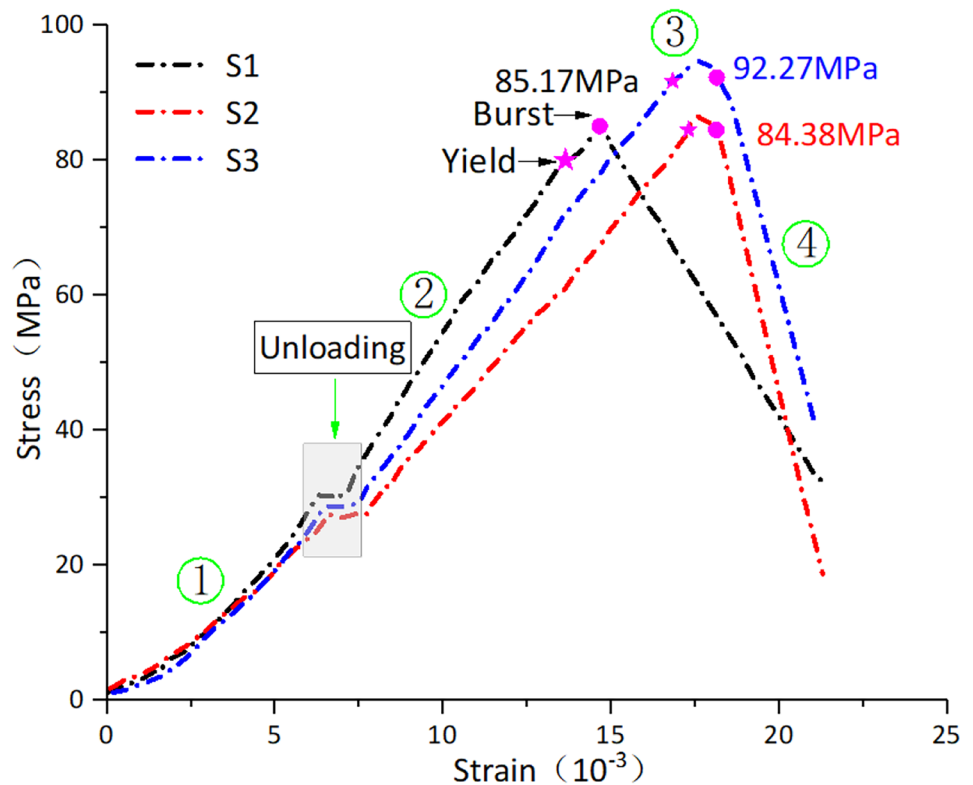


Fig. 7 Axial stress–strain curve



new microcracks began to sprout in the sandstone, and cracks continued to expand with an increase in stress until rock failure and rockburst occurred. Because many microcracks were generated in the yield stage, the AE equipment monitored many AE signals. It was easier to obtain precursor information of rockbursts at this stage. As shown in Table 3, the percentages of the axial yield point stress of sandstones S-1, S-2, and S-3 in the peak stress are 93.46, 96.11, and 95.97%, respectively, and their average axial peak stress is 88.7 MPa.

**Microfracture evolution characteristics**

During the loading and unloading in sandstone true triaxial rockburst experiments, much microfracture information is generated, including time, space, and strength (*t, x, y, z, E*) parameters, that reflect the development frequency, three-dimensional spatial position, and fracture scale (energy) of

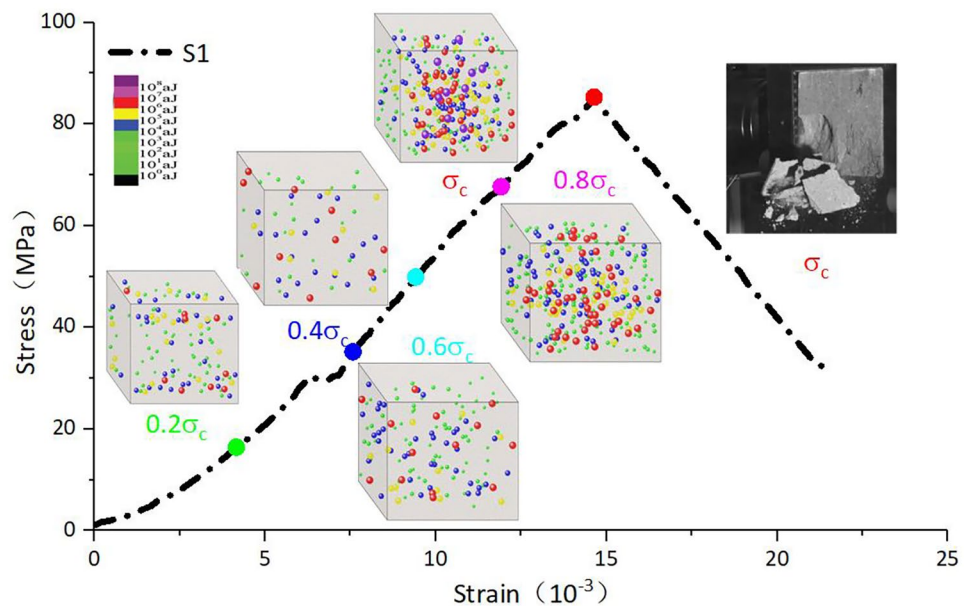
microcracks in the sandstone rockburst evolution process. Studying the spatial evolution of microcracks during rockburst experiments helps to identify the precursors of rockbursts. The AE localization algorithm uses the least-squares method combined with the Geiger localization method to iteratively approximate the source coordinates of the fracture event that meet the localization accuracy (Li et al. 2010). The absolute energy index of AE is used for the energy of a fracture event, the actual index to measure the local fracture of rock materials (Petružálek et al. 2020).

The number of microfracture events before the peak of the S-1 sample reached 1624, which revealed the temporal and spatial development law of microfracture events during the evolution of sandstone rockburst under different stress stages to the greatest extent. The S-1 sample was taken as an example for the analysis. Figure 8 shows the temporal and spatial evolution of the stress and microfracture events during the loading and unloading processes of the S-1 sandstone rockburst experiment. At 20%  $\sigma_c$ , a few events appeared in the transition region of the compaction stage, which were located at the upper and lower ends, and the event energy was relatively small. It was proved that the initial fracture scale of sandstone was small, and damage degree was low. The spatial distribution was considerably random and related to the primary fractures of the sandstone. At 40%  $\sigma_c$ , few AE localization events occurred during the elastic stage. A few events with higher

Table 3 Axial stress parameters of sandstone rockburst experiment

Sample	Axial stress yield point as a percentage of peak stress/%	Axial peak stress/MPa	Average peak stress/MPa
S-1	93.46	85.17	88.78
S-2	96.11	86.36	
S-3	95.97	94.82	

**Fig. 8** Evolution characteristics of microfracture events with stress–strain during rockburst experiment



energy levels appeared near the sandstone face owing to the completion of the rapid unloading. At 60%  $\sigma_c$ , there were more high-energy-level red localization events in the sandstone than in the previous stage, mainly distributed near the sandstone surface and less in the center. At 80%  $\sigma_c$ , many high-energy-level events were observed in the central part of the sandstone and near the airside surface. In a comprehensive comparison, the area where the high-energy event (red hypocenter ball) occurred was the gathering location of the low-energy events in the previous stage. This indicates that the development of cracks of different sizes before and after had an associated causal relationship. Large-scale cracks were caused by small-scale crack propagation and concentrated penetration. When  $\sigma_c$  was reached, rockbursts occurred, and the sandstone localization event appeared as a high-energy purple event mainly distributed in the center of the sandstone sample, indicating that the sandstone was destroyed. The high-energy-level events were located in the middle and lower parts where the rockburst fragments were ejected. Therefore, with the increase in loading stress, high-energy events inside the sandstone gradually increased, while the high-energy events shifted to the center of the sandstone. When a large number of high-energy-level events appear in a sandstone specimen, there is sizable internal damage, and the sandstone may be about to be destroyed, leading to a rockburst. With many high-energy-level events, this stage can be used as a precursor for rockburst information.

### Stress– $RA/AF$ evolution characteristics

The AE  $RA$  and  $AF$  values can characterize the crack types of rocks during loading and unloading, where  $RA$  is defined

as the rise time divided by the amplitude of the AE signal.  $AF$  is the count of AE ringing above the threshold divided by the impact duration in kilohertz. When the  $AF$  value of the AE signal is low and  $RA$  value is high, shear cracks are mainly generated inside the rock, and vice versa, indicating the generation of tensile cracks (Wu et al. 2020). Figure 9 shows the time–stress and  $RA/AF$  evolution characteristics of the three groups of experiments. The figure reveals that the evolution characteristics are similar. The S-1, S-2, and S-3 rock samples accounted for 16.5, 17.9, and 19.4% of the sum of  $RA$  and  $AF$ , respectively, indicating that the tensile failure form was dominant in the sandstone rockburst evolution process. Generally, when  $RA/AF$  increases suddenly, the rock enters the violent destruction stage.

As shown in Fig. 9, during the loading process in the rockburst experiment, the peak strength of the S-1 sample was 85.17 MPa, and the corresponding strength of the maximum AE  $RA/AF$  parameter was 81.73 MPa, reaching 95% of the peak strength. The peak strength of the S-2 sample was 86.36 MPa, and the corresponding strength of the maximum AE  $RA/AF$  parameter was 82.25 MPa, reaching 95.24% of the peak strength. The peak strength of S-3 was 94.82 MPa, and the corresponding strength of the maximum AE  $RA/AF$  parameter was 89.45 MPa, reaching 94.34% of the peak strength. All three groups of rock samples reached more than 90% of their peak strengths. At this time, the rock samples almost entered the yield stage, new microcracks were continuously generated and expanded, and the rock samples were severely damaged. The figure shows that there was a sudden increase in  $RA/AF$  at the rapid unloading point, indicating that a large number of microcracks were generated in the sandstone owing to the rapid unloading under high pressure.



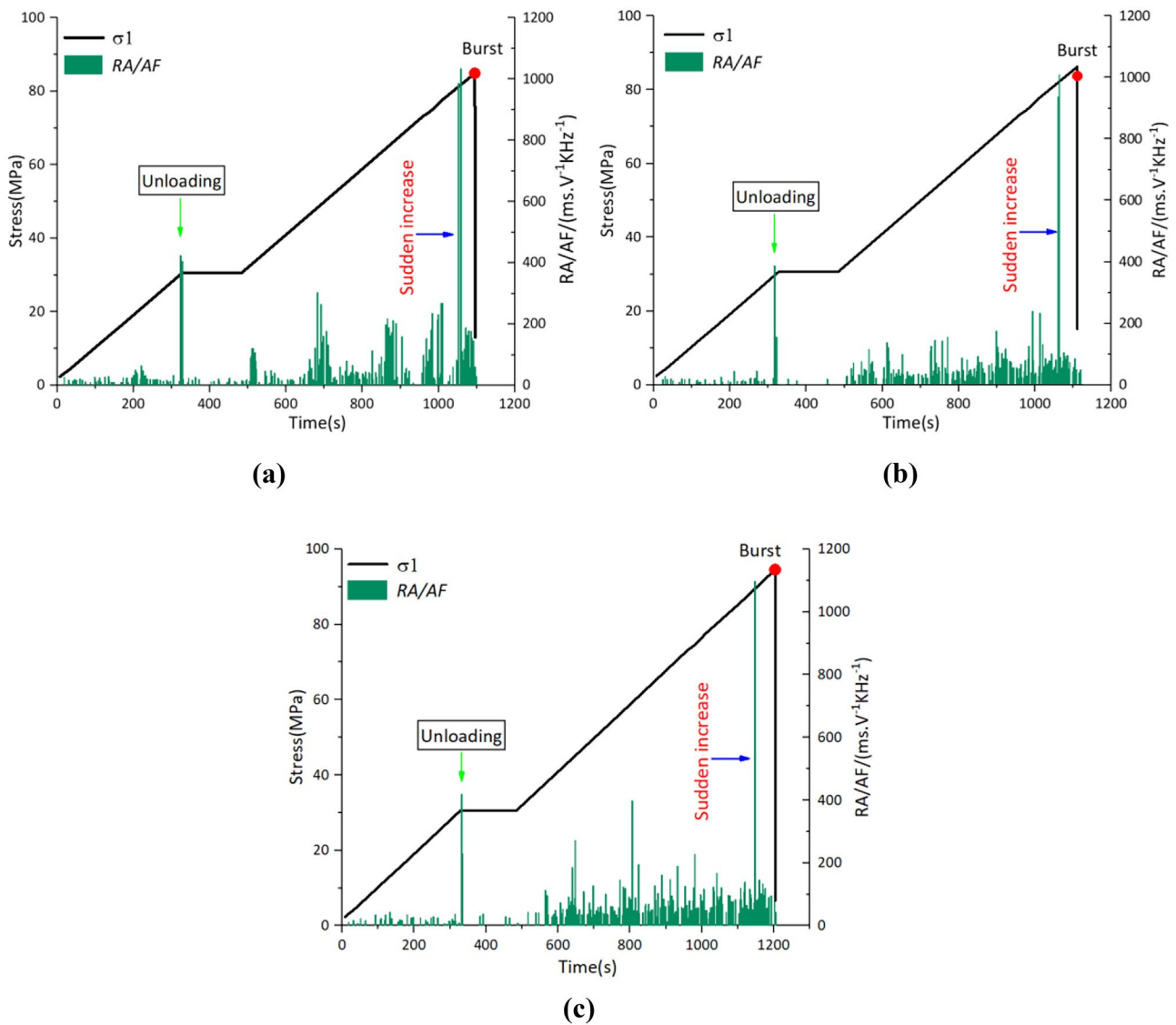


Fig. 9 Time stress and *RA/AF* evolution characteristics. **a** Sample S-1, **b** sample S-2, and **c** sample S-3

**Critical slowing-down characteristics**

**Influence of window length and lag step on critical slowing**

To calculate the variance and autocorrelation coefficient of the critical-slowing phenomenon, it is necessary to first determine the appropriate window and lag lengths. The window length is the selected sequence containing a specific amount of data, and lag length is the lag from the sequence with a specific amount of data to another new sequence with the same window length, as shown in Fig. 10. The variance is the variance of the new sequence after the lag length, and the autocorrelation coefficient is the correlation between the selected window length sequence and the new sequence obtained by the fixed lag length (Kong et al. 2015).

Taking the *RA/AF* value of the S-2 rock sample as an example, the influences of different window lengths and lag steps on the critical-slowing phenomenon were analyzed.

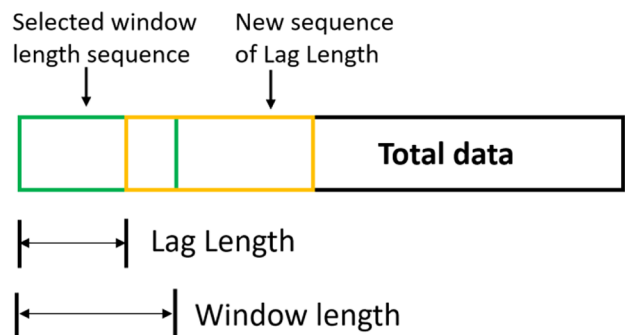
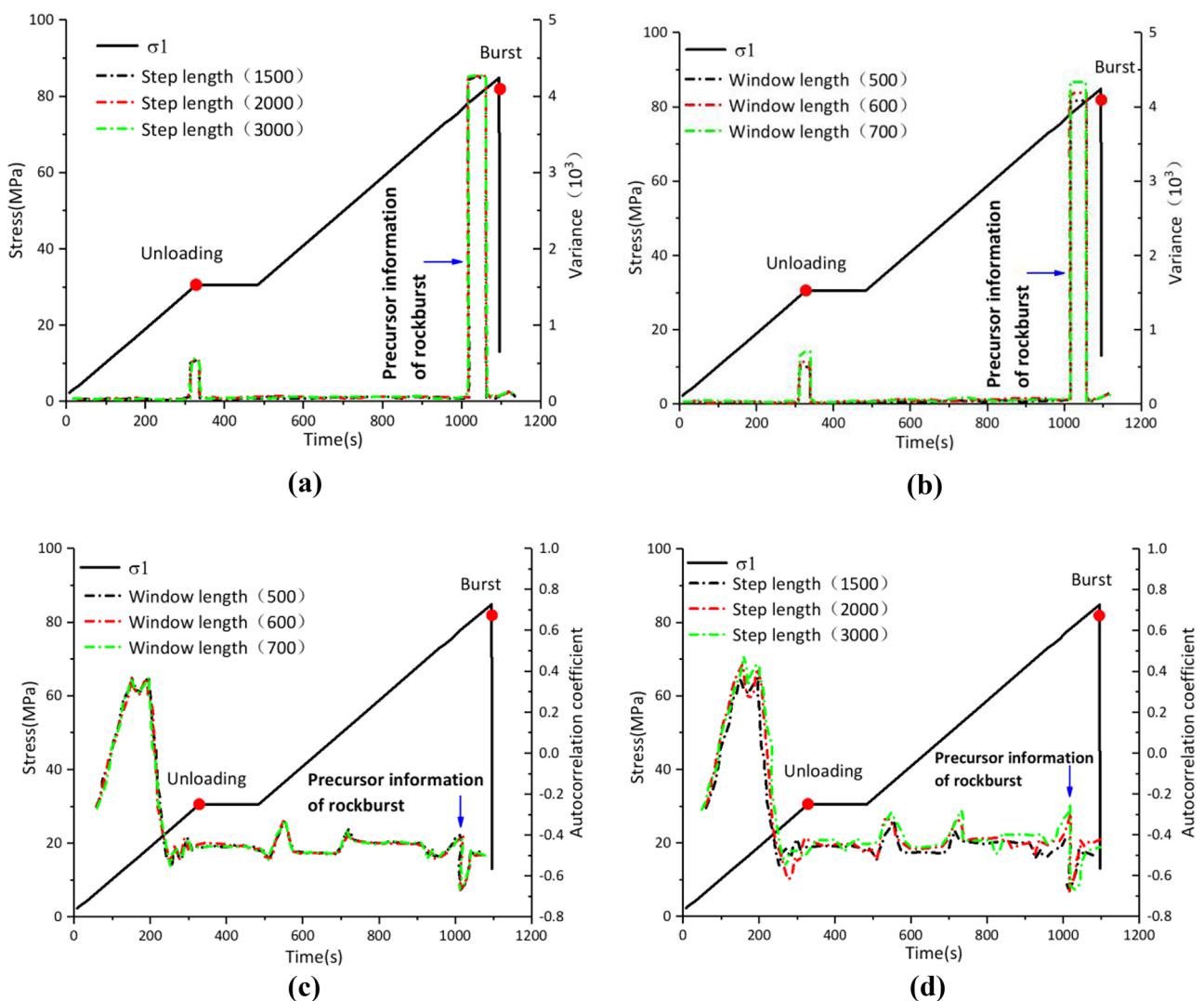


Fig. 10 Window length and lag length

The influence of different lag steps on the variance and autocorrelation coefficient was studied under the condition that the window remained unchanged; the window length was set to 500, and lag steps were 1500, 2000, and 3000. Additionally, the influence of different window lengths on the AE variance and autocorrelation coefficient was studied; the window lengths were 500, 600, and 700; and the lag step size was 1500. As shown in Fig. 11, (1) when the window length was fixed at 500 and the lag steps were 1500, 2000, and 3000, the variance increase time almost coincided (Fig. 11a). When the lag step was 1500 and the window length was 500, the precursory signal variance was largest. When the window lengths were 600 and 700, the precursory information variance decreased (Fig. 11b). Although

different window lengths and lag steps affected the variance value, the appearance times of the precursor points were the same, indicating that the influence of window lengths and lag steps on AE variance precursors can be ignored. (2) When the lag step was 1500 and window lengths were 500, 600, and 700, the autocorrelation coefficients almost coincided (Fig. 11c). When the window length was 500 and the lag step was 1500, the autocorrelation coefficient fluctuated the most. When the window length was 500 and the lag steps were 2000 and 3000, the fluctuation of the autocorrelation coefficient was relatively small (Fig. 11d). The autocorrelation coefficient was chaotic compared with the variance, but its fluctuation trend was similar. In summary, the influences of the window length and lag step on precursory information



**Fig. 11** Characteristics of critical slowing-down phenomenon under different window lengths and lag steps. **a** The window length is 500, and the lagging step size is 1500, 2000, and 3000, the influence on the variance; **b** the window length is 500, and the lagging step size is 1500, 2000, and 3000, the influence on the autocorrelation coefficient;

**c** the window length is 500, 600, and 700, and the lagging step is 1500, the influence on variance; and **d** the window length is 500, 600, and 700, and the lagging step is 1500, the influence on autocorrelation coefficient

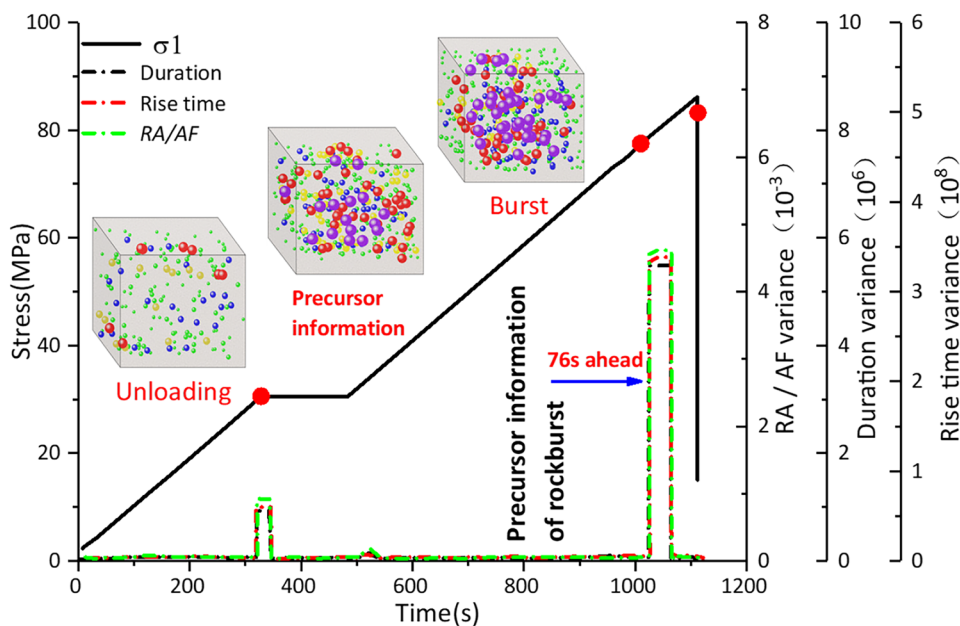
can be ignored when analyzing AE parameters during rockbursts based on the critical-slowing theory.

**Critical slowing of AE RA/AF, duration, and rise time**

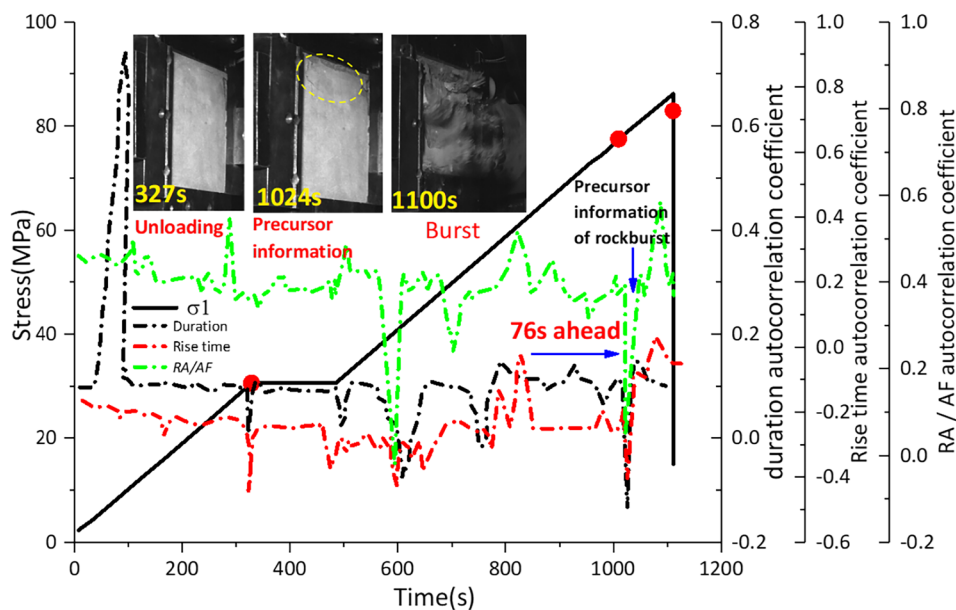
The above analysis demonstrates that the window length and lag step have little influence on the occurrence time of rockburst precursor points, which can be ignored. Therefore, the AE RA/AF value, duration, and rise time of three groups of sandstone samples were analyzed with a window length of

500 and a lag step of 1500. An attempt was made to determine whether the autocorrelation coefficient and variance of the above parameters can be taken as precursory information of sandstone rockburst failure under critical-slowing theory. Figure 12 shows the critical slowing of multiple AE parameters of sample S-3. In the variance characteristics in Fig. 12a, the AE positioning of sandstone at the unloading, precursor, and rockburst points is also shown. The autocorrelation coefficient characteristic curve in Fig. 12b shows a high-speed camera recording pictures of the unloading, precursor information,

**Fig. 12** Critical slowing of AE multiple parameters. **a** Variance and **b** autocorrelation coefficient



(a)



(b)

**Table 4** Precursory information time

Sample	Precursory time (s)	Rockburst time (s)	Early warning time (s)	Average early warning time (s)	Early warning time percentage (%)	Average alert time advance percentage (%)
S-1	1052	1097	45		95.9	
S-2	1063	1111	48	56.3	95.6	94.9
S-3	1024	1100	76		93.1	

and rockburst points. The characteristic information of the instability precursors of the other rock samples is presented in Table 4. The table shows that the precursory information of the three groups of sandstone samples appeared before the rockburst. The rockburst time in this study was subject to the time recorded by the high-speed camera. In the three groups of experiments, only sample S-1 experienced rockbursts at the time of the axial peak stress; samples S-2 and S-3 experienced rockbursts after the axial peak stress.

For sample S-3 (Fig. 12), the variance and autocorrelation coefficient curves of the AE  $RA/AF$  value, duration, and rise time had the following characteristics. The variance calculated based on the critical-slowness theory was almost stable before the rock phase state changes. When the rock changed from one phase state to another, a dispersion fluctuation phenomenon occurred at the critical point. The fluctuation of sandstone at the rapid unloading point is considered to have been caused by a large number of microcracks in the sandstone resulting from rapid unloading under true triaxial high-pressure loading. The corresponding AE localization shows that these microcracks are mainly distributed near the free face. The image captured by the high-speed camera shows that there were no cracks on the sandstone surface at this time. Significant variance fluctuation occurred near the rockburst failure. The AE localization event showed that many high-energy events occurred in the sandstone at this time. The high-speed photographs also show cracks in the sandstone, indicating that the rockburst occurred immediately. As shown in Fig. 12a, the variance curve trend and shape of the AE  $RA/AF$  value, rise time, and duration parameters are similar, and the takeoff points are highly consistent on the time scale. As shown in Fig. 12b, the fluctuation of the autocorrelation coefficient was relatively chaotic compared with the variance, resulting in more false signals. The variance was more straightforward than the autocorrelation coefficient of the precursor information. Therefore, the variance and autocorrelation coefficient can be considered the main and auxiliary criterion of the precursory information of rockbursts, respectively.

As shown in Table 4, the rockburst precursor of the sample S-1 appeared at 1052 s, the rockburst time was 1097 s, and the rockburst warning time advanced by 45 s. The rockburst precursor of the sample S-2 appeared 1063 s, the rockburst time was 1111 s, and the rockburst warning time advanced by 48 s. The rockburst precursor of sample

S-3 appeared at 1024 s, the rockburst time was 1100 s, and the rockburst warning time advanced by 76 s. The precursory information of rockbursts in the three groups of tests appeared in the yield stage, which is the stage of microcrack initiation. Therefore, the precursory information on critical slowing at this stage is of research value.

## Conclusions

A rockburst experimental system was developed to conduct true triaxial unloading rockburst experiments. Critical-slowness theory was used to study the AE signal precursor information in the rockburst process. The following conclusions were drawn:

1. An unloading platform appeared in the stress–strain curve at the unloading point. It is believed that the unloading platform of the stress–strain curve results from the rapid unloading of sandstone in the true triaxial loading direction, and the sandstone sample expands rapidly in the unloading direction. Owing to the Poisson effect, the axial direction of the sandstone sample is shortened. A recording by a high-speed camera shows that the occurrence time of a rockburst does not necessarily correspond to the peak stress point of the stress–strain curve.
2. In the early stage of a rockburst, critical slowing occurs at the crucial point, manifested by increased variance and autocorrelation coefficients. During rapid unloading, the variance and autocorrelation system increases. This may be caused by the large number of cracks generated during unloading. The window length and lag step size have little influence on the appearance time of the precursory characteristics of the AE variance. However, they significantly influence the stationarity of the autocorrelation coefficient.
3. The variances of the AE  $RA/AF$  value, duration, and rise time are the same. The sudden change time of the precursor signal is also same, the waveform fluctuation is similar, and they all appear before the rockburst. The AE localization events show that many high-energy events occur in the sandstone at this time, and cracks appear on the sandstone surface. The autocorrelation coefficient fluctuates significantly compared with the variance;



therefore, the variance can be regarded as the primary precursor information of rockbursts.

**Funding** This research was supported by the National Natural Science Foundation of China (Grant Nos. 41941018 and 52074299), Fundamental Research Funds for the Central Universities (Grant No. 2021JCCXS03), and Program of China Scholarship Council (202006430049).

## Declarations

**Conflict of interest** The authors declare no competing interests.

## References

- Beck KK, Fletcher MS, Gadd PS (2018) Variance and rate-of-change as early warning signals for a critical transition in an aquatic ecosystem state: a test case from Tasmania, Australia. *J Geophys Res-Biogeosci* 123(2):495–508. <https://doi.org/10.1002/2017JG004135>
- Cook NGW (1963) The basic mechanics of rockbursts. *J S Afr I Min Metall* 64(3):71–81
- Dakos V, Scheffer M (2008) Slowing down as an early warning signal for abrupt climate change. *Proc Natl Acad Sci* 105(38):14308–14312. <https://doi.org/10.1073/pnas.0802430105>
- Dong L, Chen Y, Sun D (2021) Implications for rock instability precursors and principal stress direction from rock acoustic experiments. *Int J Min Sci Technol* 31(5):789–798. <https://doi.org/10.1016/j.ijmst.2021.06.006>
- Du K, Tao M, Li X (2016) Experimental study of slabbing and rockburst induced by true-triaxial unloading and local dynamic disturbance. *Rock Mech Rock Eng* 49(9):3437–3453. <https://doi.org/10.1007/s00603-016-0990-4>
- Gong F, Luo Y, Li X (2018) Experimental simulation investigation on rockburst induced by spalling failure in deep circular tunnels. *Tunn Undergr Sp Tech* 81:413–427. <https://doi.org/10.1016/j.tust.2018.07.035>
- Gong FQ, Wu C, Luo S (2019) Load–unload response ratio characteristics of rock materials and their application in prediction of rockburst proneness. *Bull Eng Geol Environ* 78(7):5445–5466. <https://doi.org/10.1007/s10064-019-01474-6>
- Gong F, Luo S, Jiang Q (2022) Theoretical verification of the rationality of strain energy storage index as rockburst criterion based on linear energy storage law. *J Rock Mech Geotech*. <https://doi.org/10.1016/j.jrmge.2021.12.015>
- Gopalakrishnan EA, Sharma Y, John T (2016) Early warning signals for critical transitions in a thermoacoustic system. *Sci Rep* 6(1):1–10. <https://doi.org/10.1038/srep35310>
- Hardy HR (1972) Application of acoustic emission techniques to rock mechanics research. *Acoustic Emission, ASTM STP* 505:41–83
- He MC, Nie W, Zhao ZY (2012) Experimental investigation of bedding plane orientation on the rockburst behavior of sandstone. *Rock Mech Rock Eng* 45(3):311–326. <https://doi.org/10.1007/s00603-011-0213-y>
- He MC, Ren FQ, Cheng C (2019) Experimental and numerical analyses on the effect of stiffness on bedded sandstone strain burst with varying dip angle. *Bull Eng Geol Environ* 78(5):3593–3610. <https://doi.org/10.1007/s10064-018-1363-x>
- He MC, Li JY, Liu DQ (2020) Latest progress of research on rockburst experiment mechanism and its control. *IOP Conf Ser Earth Environ Sci* 570(3):032033 (IOP Publishing)
- He MC, Li JY, Liu DQ (2021) A novel true triaxial apparatus for simulating strain bursts under high stress. *Rock Mech Rock Eng* 54(2):759–775. <https://doi.org/10.1007/s00603-020-02285-y>
- Kaiser PK, Cai M (2012) Design of rock support system under rockburst condition. *J Rock Mech Geotech* 4(3):215–227. <https://doi.org/10.3724/SP.J.1235.2012.00215>
- Kong X, Wang E, Hu S (2015) Critical slowing down on acoustic emission characteristics of coal containing methane. *J Nat Gas Sci Eng* 24:156–165. <https://doi.org/10.1016/j.jngse.2015.03.020>
- Li Z, Xu R (2021) An early-warning method for rock failure based on Hurst exponent in acoustic emission/microseismic activity monitoring. *Bull Eng Geol Environ* 80(10):7791–7805. <https://doi.org/10.1007/s10064-021-02446-5>
- Li YH, Liu JP, Zhao XD (2010) Experimental studies of the change of spatial correlation length of acoustic emission events during rock fracture process. *Int J Rock Mech Min* 47(8):1254–1262. <https://doi.org/10.1016/j.ijrmms.2010.08.002>
- Li H, Qiao Y, Shen R (2021) Effect of water on mechanical behavior and acoustic emission response of sandstone during loading process: phenomenon and mechanism. *Eng Geol* 294:106386. <https://doi.org/10.1016/j.enggeo.2021.106386>
- Liu X, Liang Z, Zhang Y (2018) Experimental study on the monitoring of rockburst in tunnels under dry and saturated conditions using AE and infrared monitoring. *Tunn Undergr Sp Tech* 82(2018):517–528. <https://doi.org/10.1016/j.tust.2018.08.011>
- Liu D, Ling K, Guo C (2022) Experimental simulation study of rockburst characteristics of Sichuan-Tibet granite: a case study of the Zheduoshan tunnel. *Eng Geol* 305:106701. <https://doi.org/10.1016/j.enggeo.2022.106701>
- Lockner D (1993) The role of acoustic emission in the study of rock fracture. *Int J Rock Mech Min Sci Geomech Abstr* 30(7):883–899. [https://doi.org/10.1016/0148-9062\(93\)90041-B](https://doi.org/10.1016/0148-9062(93)90041-B) (Pergamon)
- Luo D, Xie Y, Lu S (2022) Experimental study on the effects of water saturation on the microseismic and acoustic emission characteristics of sandstone in different stress states. *Rock Mech Rock Eng* 55:6583–6603. <https://doi.org/10.1007/s00603-022-03001-8>
- Petružálek M, Jechumtálová Z, Šílený J (2020) Application of the shear-tensile source model to acoustic emissions in Westerly granite. *Int J Rock Mech Min* 128:104246. <https://doi.org/10.1016/j.ijrmms.2020.104246>
- Ramos O (2010) Criticality in earthquakes. Good or bad for prediction? *Tectonophysics* 485(1–4):321–326. <https://doi.org/10.1016/j.tecto.2009.11.007>
- Scheffer M, Bascompte J, Brock WA (2009) Early-warning signals for critical transitions. *Nature* 461(7260):53–59. <https://doi.org/10.1038/nature08227>
- Venegas JG, Winkler T, Musch G (2005) Self-organized patchiness in asthma as a prelude to catastrophic shifts. *Nature* 434(7034):777–782. <https://doi.org/10.1038/nature03490>
- Wang CL, Cao C, Liu Y (2021) Experimental investigation on synergetic prediction of rockburst using the dominant-frequency entropy of acoustic emission. *Nat Hazards* 108(3):3253–3270. <https://doi.org/10.1007/s11069-021-04822-6>
- Wang CL, Cao C, Li C (2022) Experimental investigation on synergetic prediction of granite rockburst using rock failure time and acoustic emission energy. *J Cent South Univ* 29(4):1262–1273. <https://doi.org/10.1007/s11771-022-4971-3>
- Wei Y, Li Z, Kong X (2018) The precursory information of acoustic emission during sandstone loading based on critical slowing down theory. *J Geophys Eng* 15(5):2150–2158. <https://doi.org/10.1088/1742-2140/aac009>
- Wu SH, Gan YX, Ren Y (2020) Feasibility research of AE monitoring index in tunnel based on RA and AF. *Chin J Eng* 42(6):723–730 (in Chinese)
- Wu C, Gong F, Luo Y (2021) A new quantitative method to identify the crack damage stress of rock using AE detection parameters.

- Bull Eng Geol Environ 80(1):519–531. <https://doi.org/10.1007/s10064-020-01932-6>
- Yang J, Lu W, Jiang Q (2016) A study on the vibration frequency of blasting excavation in highly stressed rock masses. *Rock Mech Rock Eng* 49(7):2825–2843. <https://doi.org/10.1007/s00603-016-0964-6>
- Zhang X, Li Z, Niu Y (2019) An experimental study on the precursory characteristics of EP before sandstone failure based on critical slowing down. *J Appl Geophys* 170:103818. <https://doi.org/10.1016/j.jappgeo.2019.103818>
- Zhang Z, Li Y, Hu L (2021) Predicting rock failure with the critical slowing down theory. *Eng Geol* 280:105960. <https://doi.org/10.1016/j.enggeo.2020.105960>
- Zhu X, Tang Y, Fan J (2022) Experimental study on failure precursors of fine sandstone based on critical slowing down theory. *Chin J Rock Mech Eng* 41(1):9 (in Chinese)

Springer Nature or its licensor (e.g. a society or other partner) holds exclusive rights to this article under a publishing agreement with the author(s) or other rightsholder(s); author self-archiving of the accepted manuscript version of this article is solely governed by the terms of such publishing agreement and applicable law.